

Article

A Theoretical Study of the Oxygen Release Mechanisms of a Cu-Based Oxygen Carrier during Chemical Looping with Oxygen Uncoupling

Minjun Wang ^{1,*}, Shixiong Zhang ¹, Ming Xia ² and Mengke Wang ¹

¹ School of Energy and Power, Jiangsu University of Science and Technology, Zhenjiang 212003, China; zsx4920816@163.com (S.Z.); wangmk0607@163.com (M.W.)

² Chuzhou Cigarette Factory, China Tobacco Anhui Industrial Co., Ltd., Chuzhou 239000, China; xiaming198708@126.com

* Correspondence: wmj403@just.edu.cn

Abstract: The Cu-based oxygen carrier is a promising material in the chemical looping with oxygen uncoupling (CLOU) process, while its performance in the CLOU is significantly dependent on the oxygen release properties. However, the study of oxygen release mechanisms in CLOU is not comprehensive enough. In this work, the detailed oxygen release mechanisms of CuO(110) and CuO(111) are researched at an atomic level using the density functional theory (DFT) method, including the formation of O₂, the desorption of O₂ and the diffusion of O anion, as well as the analysis of the density of states. The results show that (1) the most favorable pathway for O₂ formation and desorption occurs on the CuO(110) surface of O-terminated with energy barriers of 1.89 eV and 3.22 eV, respectively; (2) the most favorable pathway for O anion diffusion occurs in the CuO(110) slab with the lowest energy barrier of 0.24 eV; and (3) the total density of states for the O atoms in the CuO(110) slab shifts to a lower energy after an O vacancy formation. All of the above results clearly demonstrate that the CuO(110) surface plays a significantly important role in the oxygen release reaction, and the oxygen vacancy defect should be conducive to the reactivity of oxygen release in a Cu-based oxygen carrier.

Keywords: chemical looping with oxygen uncoupling; Cu-based oxygen carrier; oxygen release mechanisms; density functional theory



Citation: Wang, M.; Zhang, S.; Xia, M.; Wang, M. A Theoretical Study of the Oxygen Release Mechanisms of a Cu-Based Oxygen Carrier during Chemical Looping with Oxygen Uncoupling. *Catalysts* **2022**, *12*, 332. <https://doi.org/10.3390/catal12030332>

Academic Editor: Albert Poater

Received: 2 February 2022

Accepted: 14 March 2022

Published: 15 March 2022

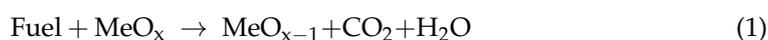
Publisher's Note: MDPI stays neutral with regard to jurisdictional claims in published maps and institutional affiliations.



Copyright: © 2022 by the authors. Licensee MDPI, Basel, Switzerland. This article is an open access article distributed under the terms and conditions of the Creative Commons Attribution (CC BY) license (<https://creativecommons.org/licenses/by/4.0/>).

1. Introduction

Carbon emissions from fossil fuel utilization are important sources of greenhouse gases (GHGs) that cause the greenhouse effect [1]. To minimize global CO₂ emissions, it is critical to develop effective CO₂ capture technologies [2]. Chemical looping combustion (CLC) is a potential approach for capturing 100% carbon from fuel at a cheap cost and with low energy penalties [3]. A two-step reaction can be characterized as the CLC process: (i) the fuel is oxidized in the fuel reactor (FR) by an oxygen carrier, usually a metal oxide, to produce a concentrated stream of H₂O and CO₂. (ii) The reduced oxygen carrier is then re-oxidized by air in an air reactor (AR) in the next step. The oxidized carrier is then separated and transferred to the fuel reactor in preparation for the next cycle [4]. Below are the simplified reaction equations for the two-step reaction.



Instead of air, the oxygen carrier is employed in CLC to carry oxygen to the fuel. As a result, the CLC has a CO₂ separation advantage over traditional combustion, where CO₂ is diluted with primary flue gas components, such as nitrogen [5]. In addition, CLC also

reduces NO_x generation because the fuel burns in the FR without air, and the oxidation of the oxygen carrier occurs at a lower temperature in the absence of fuel [6]. However, solid fuels are difficult to be applied in the traditional CLC process due to the rate-limiting gasification stage of solid fuels. To address this problem, an innovative CLC technology has been suggested, named chemical looping with oxygen uncoupling (CLOU) [7]. The CLOU technology makes use of the characteristics of particular metal oxides, which, at high temperatures, produce gaseous O₂. The CLOU process has three reaction steps: (i) the decomposition of the oxygen carrier generates gaseous O₂ in the FR; (ii) the fuel is oxidized by the oxygen carrier in the FR; and (iii) the reduced oxygen carrier is re-oxidized by air in the AR. The simplified reaction equations of CLOU are shown below.



The gaseous O₂ generated by the oxygen carrier in the CLOU process significantly speeds up the conversion rate of solid fuels at the desired combustion temperatures (800–1000 °C) [7]. The reactivity and stability of the oxygen carrier are critical for the CLOU process applicability [7]. Many materials appropriate for CLOU have been studied to date, including perovskite-type oxides [8], natural ores [9], synthetic materials [10], and transitional metal oxides [11]. As a consequence of advanced research, transitional metal oxides in a variety of forms, such as nickel, cobalt, iron, manganese, or copper oxides, were confirmed as potential candidates for oxygen carriers [11–16]. Among these metal complexes, copper-based oxygen carriers are appealing due to their high reactivity, high oxygen capacity, and environmental friendliness [17]. On the other hand, CuO has certain drawbacks, including (i) a low mechanical strength, which may lead to defluidization, and (ii) a strong agglomeration trend, which may result in low reactivity due to its low melting point [18]. De Diego et al. [19] found that the reaction rate of CuO dropped rapidly with repeated cycles due to agglomeration and sintering.

Experimental studies revealed that using inert materials as a support for CuO can improve chemical stability and mechanical strength [20,21]. Yet, the addition of inert support inevitably reduces the oxygen transfer capacity and redox ability per unit mass. Therefore, further work has to be conducted to increase the reactivity of the Cu-based oxygen carrier in CLOU. According to the principle described above, the performance of oxygen release for oxygen carriers is a crucial issue that determines the reactivity of CLOU. Numerous experimental and theoretical studies have been conducted on the mechanisms of the reaction in CLOU [22–25]. The results show that oxygen carriers release oxygen at the solid surface, and lattice oxygen diffusion occurs at the same time; consequently, the total reaction rate is controlled by both surface reactions and bulk oxygen diffusion. When exposed to a gaseous atmosphere (reducing gases), oxygenic species on the surface of oxygen carrier react with reducing gases at specific active sites to produce the desired products. As a result of the surface reactions, surface oxygen is consumed, and an oxygen chemical potential gradient develops; oxygen anions must migrate from the bulk phase to the surface [26–28]. To achieve a high reactant conversion and improve the desired product selectivity, the control of the oxygen diffusion and the oxygen release from surface pathways is required [29–31].

Despite the fact that many experimental methods can effectively observe and track changes in bulk phase oxygen carriers, experimental technologies for studying the microscopic mechanisms of CLOU are severely limited because experimental characterization is difficult to capture and it is difficult to observe the transformation of reactants at extreme-speed time scales [32,33]. Computational simulation has demonstrated significant benefits in the research of material surface structure and characteristics, as well as chemical reaction mechanisms. In the areas of solid material structure simulation, property prediction, and an in-depth understanding of reaction mechanisms, first-principle calculations can often

provide knowledge and understanding that cannot be achieved by experiments [34–36]. In recent years, first-principles calculations have been widely used for oxygen carriers, such as NiO, Fe₂O₃, Fe₃O₄, and perovskites [31,37–41]. Meanwhile, a number of studies research Cu-based oxygen carriers by density functional theory (DFT) calculations. Zhao et al. [42] investigated the CuO–support interaction in Cu-based oxygen carriers using DFT calculations. The effects of several inert supports on the decomposition reactivity and sintering resistance of Cu-based oxygen carriers were compared. Wu et al. [43] systematically calculated the kinetic mechanisms of CO oxidation on the CuO (111) surface using the DFT calculation to consider the adsorption, reaction, and desorption processes. Zhang et al. [44] studied the decomposition mechanisms of CuO/CuAl₂O₄ and the effects of inert supports on the Cu-based oxygen carriers. The results show that the O anion migrates from the lattice to the surface and forms an O₂ complex. Zheng et al. [45] reported the detailed oxidation steps of the Cu-based oxygen carrier by DFT calculations. According to the findings, the bulk Cu₂O phase forms preferentially as a result of copper outward diffusion in the Cu(111) bulk, before being oxidized to produce the bulk CuO phase. Mishra et al. [46] correlated the oxygen vacancy creation energy of the perovskite oxygen carriers with their redox properties by DFT calculations and experiment research. The results indicate that vacancy creation energy is an effective indicator for oxygen release properties of metal oxide oxygen carriers.

Although there has been a lot of research on Cu-based oxygen carriers, the study of oxygen release mechanisms in CLOU is still not comprehensive enough. For instance, the CuO(110) surface has not been examined in CLOU, which is a significant crystal face due to the presence of active sites on it, and X-ray diffraction characterization of CuO also revealed that one of the most observed peaks relates to the (110) facet [46–51]. In addition, the current research exclusively considers O anion diffusion from the lattice to the surface. The diffusion of the O anion between the sites on the surface has not been studied. The objective of this work is to investigate the oxygen release mechanisms of the Cu-based oxygen carrier during CLOU more comprehensively. The oxygen release processes of CuO(111) and CuO(110) were simulated through DFT calculations. More O anion diffusion paths are considered. Additionally, the effects of oxygen vacancy formed during O anion migration on CuO were studied, and the oxygen vacancy creation energy in CuO was calculated. This study aims to understand the main oxygen release mechanisms and real reaction active sites of CLOU on the Cu-based oxygen carrier, which is helpful in controlling and improving the CLOU process.

2. Results and Discussion

2.1. Calculations of Bulk CuO and O₂

The calculated Cu–O bond length (0.196 nm) of the CuO agrees well with the experimental value (0.195 nm) [52]. The calculated lattice parameters for CuO are $a = 4.723 \text{ \AA}$, $b = 3.418 \text{ \AA}$, $c = 5.161 \text{ \AA}$ and $\beta = 99.34^\circ$, which is comparable to the experimental results ($a = 4.683 \text{ \AA}$, $b = 3.422 \text{ \AA}$, $c = 5.129 \text{ \AA}$ and $\beta = 99.54^\circ$) [53]. In addition, the bond length of molecule O₂ predicted using our approach is 0.124 nm, which is consistent with experimental result of 0.121 nm [54]. The above results in this investigation support the accuracy of the chosen computation method.

2.2. The Mechanisms of Oxygen Release from the CuO Surface

First, the oxygen release reaction on the CuO(110) surface was studied. In the preliminary work, the oxygen release process on the CuO(110) surface of Cu-terminated was simulated. However, the calculation results show that it is difficult to form stable O₂, probably because the oxygen atoms of the Cu-terminated surface are not in the surface layer, which is very stable, and it is difficult to break the bond with the Cu atoms and migrate to the outermost layer. Therefore, the oxygen release process on the CuO(110) surface of O-terminated is simulated and analyzed here.

The IS column in Figure 1 shows the relaxed structure of the CuO(110) surface of O-terminated. The oxygen atoms on the CuO(110) surface of O-terminated are of the same chemical type as the three-fold coordinated atoms. Yet, oxygen atoms may be in different environments and combine in different paths. O1, O2, O3, and O4 were assigned to the four oxygen atoms on the CuO(110) surface of O-terminated (see Figure 1). In order to determine the possible O₂ formation process, an O1 atom was removed and reintroduced to bond with three neighboring O atoms, including O2, O3, and O4. Subsequently, these configurations were optimized. The optimization results show that the O1 atom forms bonds with the O2, O3 and O4 atoms with bond lengths of 1.466 Å, 1.276 Å, and 1.370 Å, respectively. These bond lengths are close to those of the free O₂ molecule (1.124), implying that an O₂ complex is formed in the three structures. Therefore, the O₂ formation processes of O1-O2, O1-O3, and O1-O4 were considered and denoted by path 1 (P1), path 2 (P2), and path 3 (P3), respectively. For the calculation of O₂ formation processes, the perfect CuO(110) surface of O-terminated was set as the initial state (IS). The final structure was the stable configuration with the O₂ complex, which was denoted by the IM (intermediate state). Then, a transition state (TS) search calculation was performed. The TS structure and the corresponding energy profile for the process are shown in Figures 1 and 2. The energy barriers of the path 1, path 2, and path 3 are 1.89 eV, 4.47 eV, and 4.13 eV, respectively. In addition, all three processes are endothermic by 1.72 eV, 2.38 eV, and 1.91 eV, respectively. These results suggest relatively large differences in the three paths of O₂ formation processes.

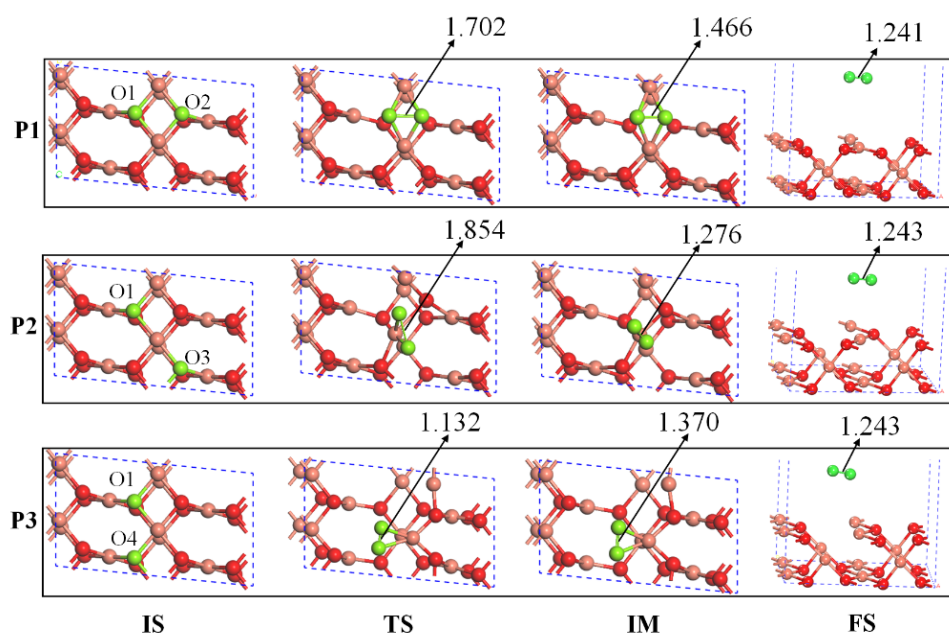


Figure 1. The initial state (IS), transition state (TS), intermediate state (IM), and final state (FS) structures for the O₂ formation and O₂ desorption processes in different pathways on the CuO(110) surface of O-terminated. The bond lengths are presented in Å. The salmon pink and red spheres denote Cu and O atoms, respectively.

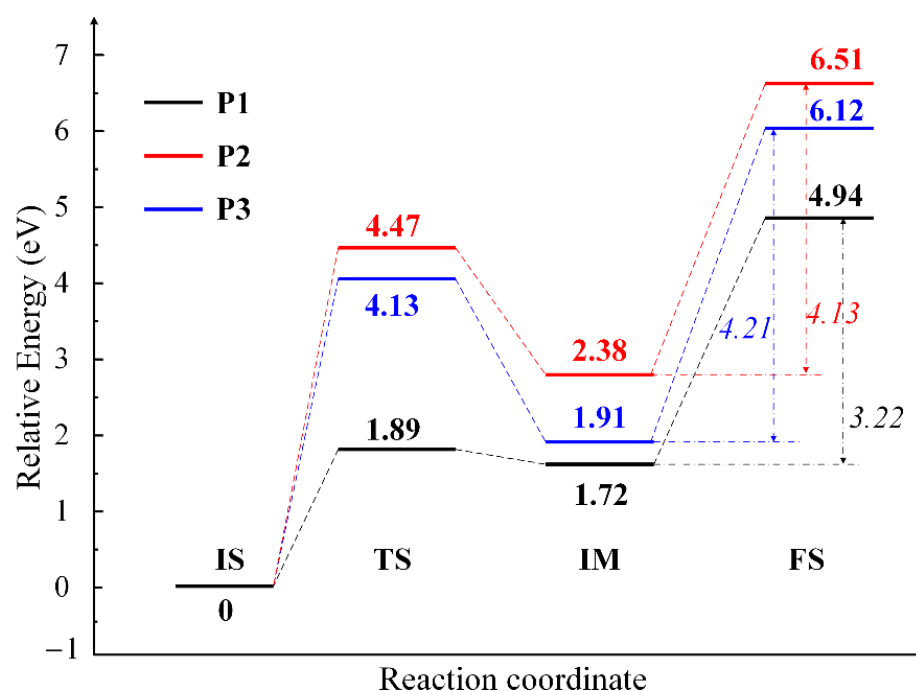


Figure 2. Potential energy diagram for the O₂ formation and desorption processes following different pathways on the CuO(110) surface of O-terminated.

Subsequently, the O₂ desorption processes following the O₂ formation were simulated. The O₂ complex formed in the intermediate state was removed and placed at a distance of 8 Å from the CuO(110) surface of O-terminated. The structures were then optimized and labeled with the FS (final state) (see Figure 1). Thus, a TS search calculation was used to determine the energy barrier between the IM and the FS. The results (see Figure 1) show that all the three O₂ desorption processes are largely endothermic by 3.22 eV, 4.13 eV, and 4.21 eV, respectively, which indicates that the oxygen is only released at high temperatures. This is consistent with the thermodynamic calculation result that the temperature of oxygen release on CuO needs to be greater than 800 °C [7]. Furthermore, due to the low energy barriers for O₂ formation and desorption, path 1 is regarded as the most favorable pathway for oxygen release on the CuO(110) surface of O-terminated. In the path 1 process, an O₂ complex is formed in the IM structure, and the O–O bond length is 1.466 Å. Then, the Cu–O bond is ruptured with a desorption energy of 3.22 eV, and the O₂ is desorbed from the CuO(110) surface. The length of the new O–O bond is 1.241 Å, which is similar to the length of a free O₂ molecule (1.240 Å).

To provide further insight into the oxygen release reaction, the density of states (DOS) was investigated. Figure 3 shows the DOS for O atoms (O1, O2), O₂ complex, and free O₂ molecule in the path 1 process, respectively. The DOS of O atoms in the IS delocalizes over a wide range due to the strong Cu–O bonds that exist in the CuO. In the IM, two peaks are observed in s orbitals, which indicates the formation of an O₂ complex. However, a large delocalization still appears in the p orbitals, which indicates that the O₂ complex still has strong interaction with the CuO(110) surface. After O₂ desorption, the DOS of O₂ in the FS was nearly the same as that of a free O₂ molecule, implying that free O₂ molecules are generated.

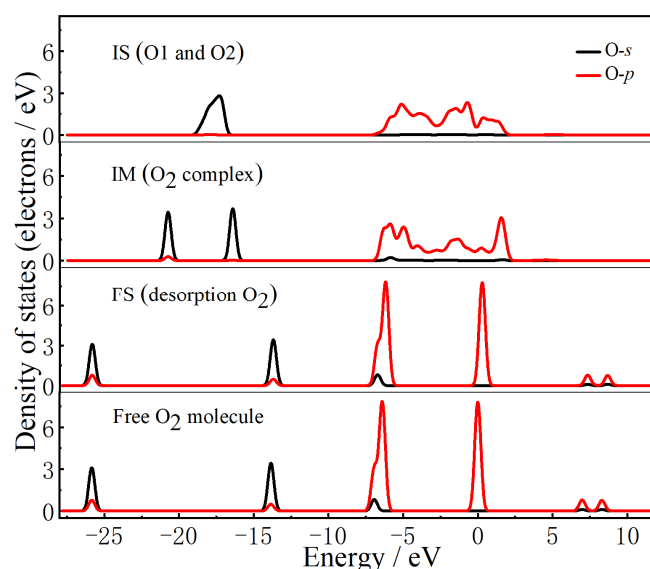


Figure 3. The DOS for O atoms (O1, O2), O₂ complex, and free O₂ molecule in the path 1 process.

Next, the oxygen release reaction on the CuO(111) surface was simulated. Of particular note, the oxygen release reaction on the CuO(111) surface was studied by the work of Zhang et al. [44]. However, the calculation methods were slightly different from those in this paper. In order to make the results in this work as comparable as possible, the O₂ formation and desorption processes were still calculated here, and the results are shown in Figures 4 and 5. There are two pathways for oxygen release on the CuO(111) surface, which are denoted as path 1 (P1) and path 2 (P2). The details of model construction are not repeated here. The energy barriers of O₂ formation in path 1 and path 2 are 3.18 eV and 2.47 eV, respectively. Both O₂ desorption processes are largely endothermic by 3.61 eV and 3.31 eV, respectively. The calculated results are quite similar to those that are reported in the literature [44] (see Table 1). Comparing the calculation results of the CuO(110) surface with that of the CuO(111) surface reveals that there is the lowest energy barrier and total energy in path 1 on the CuO(110) surface. In particular, the activation energy values of oxygen release on CuO studied by experiments (3.26 eV and 3.41 eV) [55,56] were close to the energy barrier of path 1 on the CuO(110) surface, while largely smaller than that of other pathways. The analysis above indicates that the CuO(110) surface may also play an important role in the oxygen release reaction, and the active sites in the oxygen release process on the CuO surface exist in pairs.

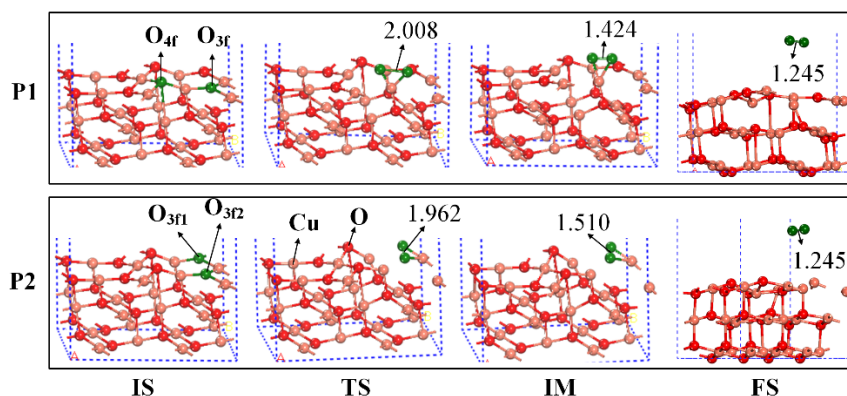


Figure 4. The initial state (IS), transition state (TS), intermediate state (IM), and final state (FS) structures for the O₂ formation and O₂ desorption processes in different pathways on the CuO(111) surface. The bond lengths are presented in Å. The salmon pink and red spheres denote Cu and O atoms, respectively.

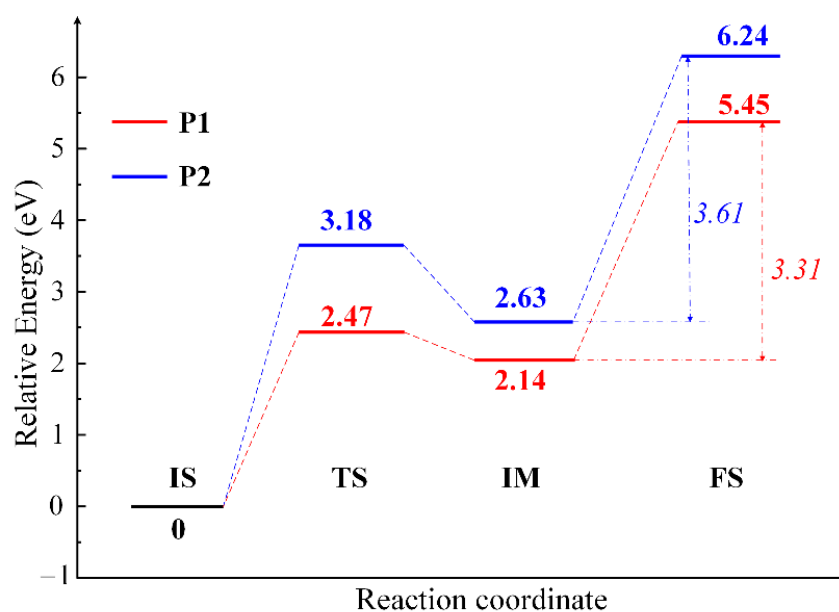


Figure 5. Potential energy diagram for the O_2 formation and desorption processes following different pathways on the CuO(111) surface.

Table 1. The energy barriers of O_2 formation (E_f), O_2 desorption (E_d), total energy (E_t), and activation energy (E_a).

	Pathway	E_f (eV)	E_d (eV)	E_t (eV)	E_a (eV)
CuO(110) surface	P1	1.89	3.22	4.94	–
	P2	4.47	4.13	6.51	–
	P3	4.13	4.21	6.12	–
CuO(111) surface	P1	2.47	3.31	5.45	–
	P2	3.18	3.61	6.24	–
CuO(111) surface in literature	P1	2.3	3.5	5.2	–
	P2	3.0	3.1	6.0	–
Experiment values	–	–	–	–	3.26
	–	–	–	–	3.41

2.3. The O Anion Diffusion Mechanisms in the CuO

As a result of the O_2 desorption from the CuO surface, surface oxygen is consumed. Therefore, oxygen anions must diffuse to the surface to maintain the oxygen release reaction. First, the O anion diffusion processes in the CuO(110) slab were studied. According to the research results of the oxygen release from CuO(110) surface, there are active sites on the surface during the oxygen release process. Thus, the O anion will diffuse to the active sites. In view of this, one active site for the O atom was labeled as O1, and the three neighboring atoms on the CuO(110) surface were labeled as O2, O3, and O4, respectively (see Figure 6).

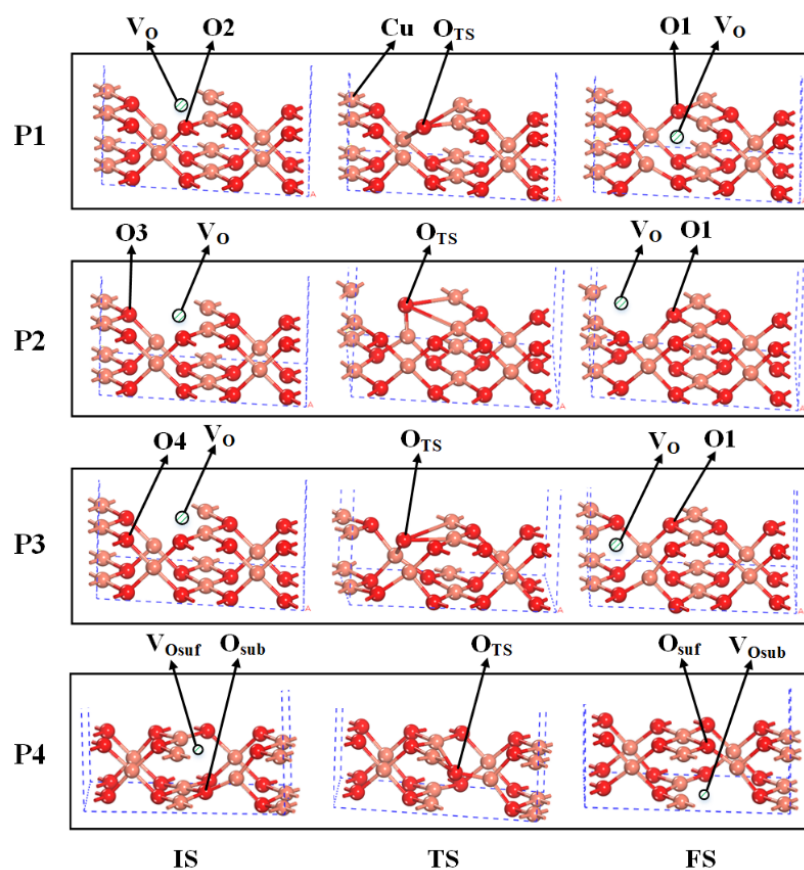


Figure 6. The initial state (IS), transition state (TS), and final state (FS) structures for the O anion diffusion processes in different pathways on the CuO(110) surface of O-terminated. The salmon pink and red spheres denote Cu and O atoms, respectively.

For this calculation, the initial state (IS) was defined as an optimized CuO(110) structure with a surface O1 vacancy. The structure CuO(110) with a surface O2 (O3 or O4) vacancy was optimized and denoted as the final state (FS). Accordingly, three O anion diffusion paths were constructed and denoted as path 1 (P1), path 2 (P2), and path 3 (P3), respectively. In addition, considering that O anion may diffuse from the lattice to the surface, the fourth pathway was constructed and denoted by path 4 (P4), in which IS was defined as an optimized CuO(110) structure with a surface oxygen vacancy (denoted as V_{O_{suf}}) and the FS was defined as an optimized CuO(110) structure with a subsurface oxygen vacancy (denoted as V_{O_{sub}}). Figures 6 and 7 show the TS search results and the corresponding energy profile for the processes. The energy barriers of path 1, path 2, path 3, and path 4 are 0.51 eV, 1.75 eV, 1.32 eV, and 0.24 eV, respectively, indicating that the energy barriers of O anion diffusion in CuO(110) are extremely low. In particular, the energy barrier of O anion diffusion in path 4 (0.24 eV) is significantly lower than that of the O₂ formation (1.89 eV, 4.13 eV, 4.47 eV) and O₂ desorption processes (3.22 eV, 4.13 eV, 4.21 eV). In addition, all the four processes are exothermic by −0.43 eV, −0.48 eV, −0.47 eV, and −0.02 eV, respectively. These results imply that O anion diffusion in CuO(110) can react readily and is energetically favorable.

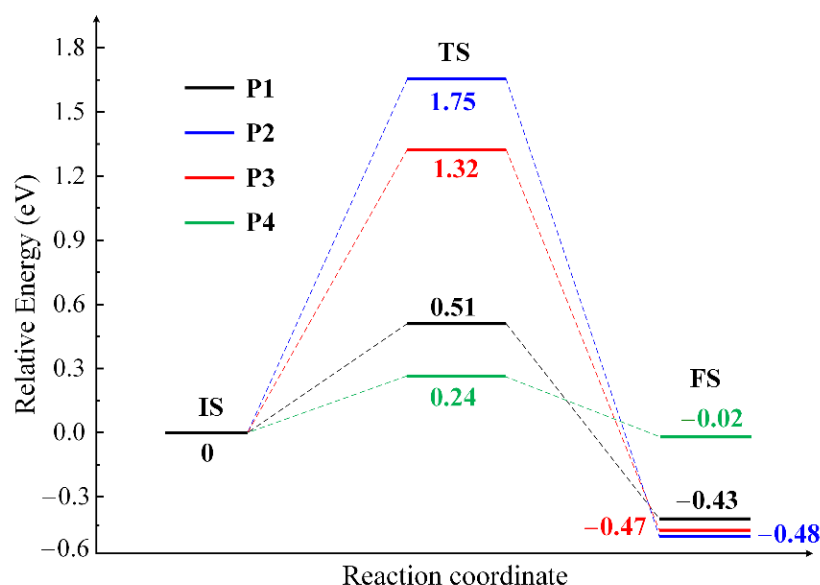


Figure 7. Potential energy diagram for the O anion diffusion processes in different pathways on the CuO(110) surface of O-terminated.

Next, the O anion diffusion processes in the CuO(111) slab were studied. The O_{4f} atom migrating to O_{3f} vacancy, O_{4f} atom migrating to O_{4f} vacancy, O_{3f} atom migrating to O_{3f} vacancy, and subsurface oxygen atom (O_{sub}) migrating to surface oxygen vacancy ($V_{O_{surf}}$) were considered as four possible O anion diffusion paths in the CuO(110) slab. Correspondingly, the four paths were denoted by path 5 (P5), path 6 (P6), path 7 (P7), and path 8 (P8), respectively. The optimized structures of IS and FS are shown in Figure 8. The reaction pathway and energy profile for the O anion diffusion in the CuO(110) slab are shown in Figures 8 and 9. The energy barriers of path 5, path 6, path 7, and path 8 are 1.67 eV, 1.58 eV, 1.16 eV, and 0.74 eV, respectively, which are also rather small. The results indicate that the O_2 formation and desorption are the rate limiting steps for oxygen release from CuO. Therefore, the key to improving the reactivity of Cu-based oxygen carriers is to decrease the energy barrier of O_2 formation and desorption processes. In addition, the average energy barrier of O anion diffusion in the CuO(111) slab is higher than that in the CuO(110) slab. Moreover, the path 5 and path 6 are endothermic by 0.40 eV and 0.28 eV, respectively. On the contrary, path 7 and path 8 are exothermic by -0.13 eV and -0.47 eV, which suggests that path 7 and path 8 are energetically favorable. In addition, the average reaction energy of O anion diffusion in the CuO(111) slab is also higher than that in the CuO(110) slab. By comparing the two slabs, path 4 in the CuO(110) slab is regarded as the most favorable pathway for O anion diffusion due to the lowest energy barrier and exothermic process. In the diffusion process of path 4, the O_{sub} atom migrates from the original location to the intermediate position between the surface and subsurface O vacancy. In addition, the subsurface Cu- O_{sub} bond is gradually rupturing. Before populating the surface oxygen vacancy, the O_{sub} atom bonds to the surface Cu atom. Given the above results, it can be found that the O anion migrates more easily in the CuO(110) slab, which further confirms the possibility that CuO(110) is important during oxygen release from the CuO. If the ratio of CuO(110) can be increased, though it is a difficult challenge, the oxygen release performance of the Cu-based oxygen carrier will be effectively improved. Nevertheless, there is a similarity between CuO(110) and CuO(111) slabs, in that paths 4 and 8 have the lowest energy barriers in their respective slabs, indicating that the O anions diffuse more easily from the lattice to the surface.

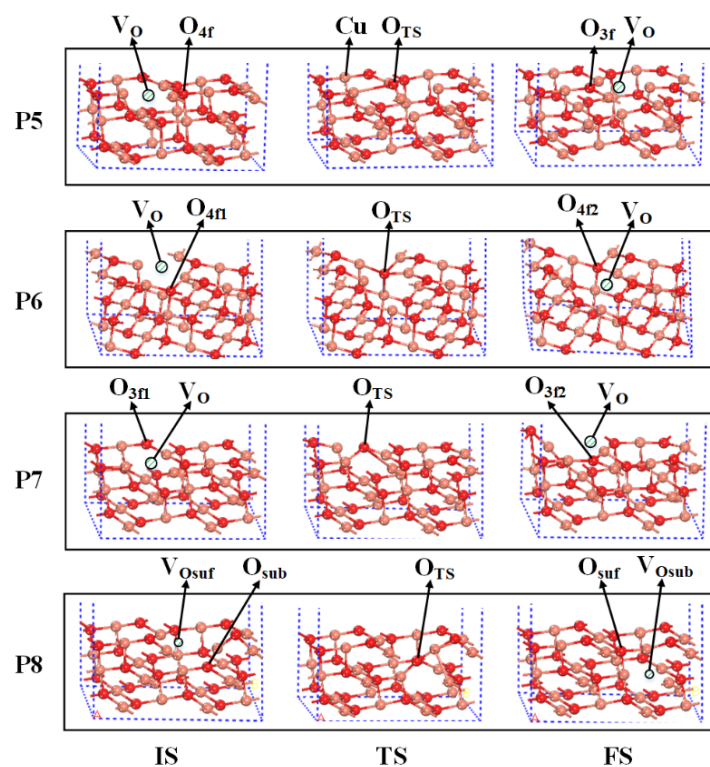


Figure 8. The initial state (IS), transition state (TS), and final state (FS) structures for the O anion diffusion processes in different pathways on the CuO(111) surface. The salmon pink and red spheres denote Cu and O atoms, respectively.

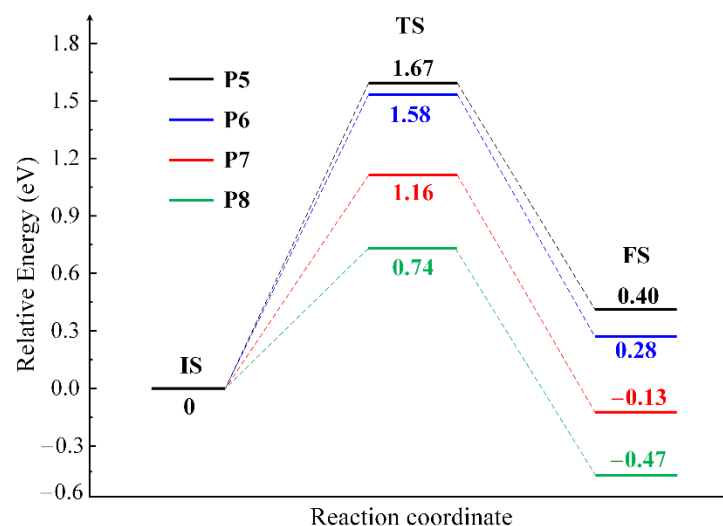


Figure 9. Potential energy diagram for the O anion diffusion processes in different pathways on the CuO(111) surface.

To provide further insight into the O anion diffusion process, the density of states in the IS, TS, and FS was investigated. The partial density of states (PDOS) of the O atom during the diffusion process in path 4 is presented in Figure 10. The electrons of the O atom in IS delocalize in a wide range near the Fermi energy level ($E_f = 0$ eV), implying that the O atom is more chemically active. In comparison to IS, the DOS of the O atom in TS has a higher peak at approximately -4.98 eV, indicating that an energy barrier is required to transition from IS to TS. In addition, the p-orbital of the O atom in FS is similar to that in IS, while the s-orbital of the O atom in FS is slightly lower than that in IS, which is consistent

with the finding that the O anion diffusion process in path 4 has an energy barrier of 0.24 eV and is exothermic by -0.02 eV.

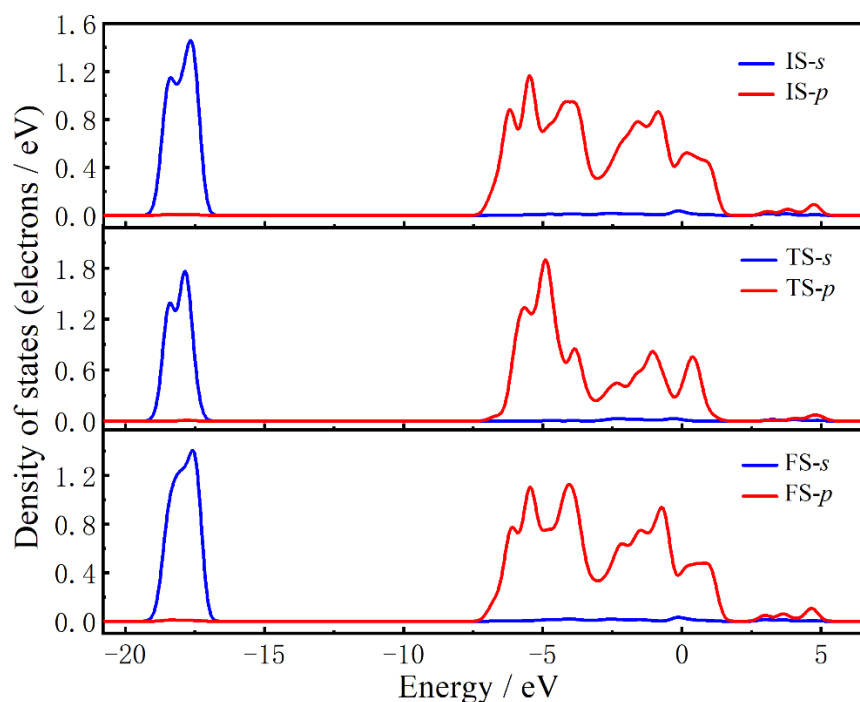


Figure 10. The partial density of states (PDOS) of the O atom during diffusion process in the path 4.

Moreover, the energy barriers of the O anion diffusion process are substantially lower than those of the O₂ formation and desorption processes, which could be caused by the O vacancy in CuO. In order to illustrate this, the density of states of the perfect CuO(110) slab and that with an O vacancy were studied. The total density of states (TDOS) and the PDOS of the O atoms are presented in Figure 11. It is observed that the TDOS for the CuO(110) slab with an O vacancy is more flat than that for the perfect CuO(110) slab, suggesting a larger delocalization in the former. In addition, for the perfect CuO(110) slab, the Cu d-orbital is hybridized with the O p-orbital as shown by the state overlap at approximately -5.84 eV and 0.10 eV, respectively. While the hybridized peaks occur at approximately -5.70 eV and 0.32 eV in the CuO(110) slab with an O vacancy. As seen from Figure 9, both hybridized peaks shift lower in energy after the formation of an O vacancy, indicating a weaker interaction of Cu with the O atom in the CuO(110) slab with an O vacancy, which facilitates O anion migration. This result may provide an idea for increasing the reactivity of oxygen release, that is, increasing oxygen vacancies. However, the oxygen vacancy creation energy in CuO was calculated to be 7.4 eV. The positive value means that energy is needed to create an oxygen vacancy in CuO.

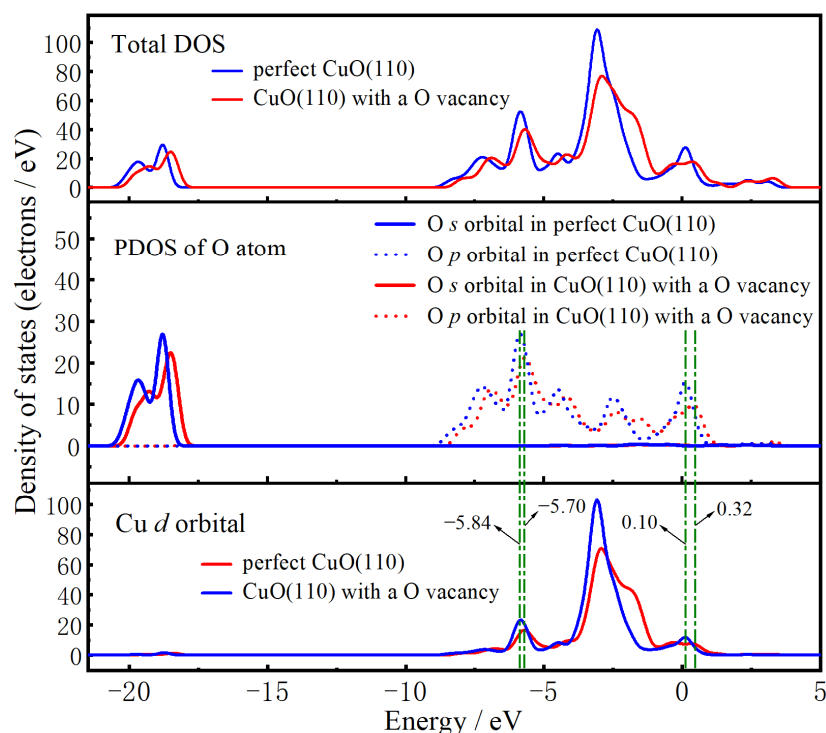


Figure 11. The TDOS of Cu(110) slab and the PDOS of the O atoms.

3. Calculation Method and Model

All DFT calculations were performed using the Cambridge Serial Total Energy Package (CASTEP) program suite [57]. Ultrasoft pseudopotentials were used to represent electron-ion interactions [58]. According to previous work conducted by our research group [47,59], the electron exchange correlation functionals of the Perdew–Wang (PW91) approximation based on the generalized gradient approximation (GGA) [60] offered the most accurate geometrical parameters of bulk CuO. As a result, the GGA-PW91 was employed to perform the calculations. The Hubbard parameter (U) was proposed for the Cu 3d orbitals to correctly reflect the high electron correlations in transition metals. We evaluated the DFT + U with U ranging from 0 to 10 eV and found that for the Cu 3d orbitals, $U = 7.5$ eV produced appropriate results. Thus, we applied $U = 7.5$ eV to the Cu 3d orbitals throughout this study. The linear/quadratic synchronous transit (LST/QST) approach [61] was used to study the transition states for each reaction.

It is critical to develop proper models for oxygen release reaction research. The unit cell of CuO that is a monoclinic structure and belongs to the $C2/c1$ space group is depicted in Figure 12. The surface of CuO(110) was modeled using the supercell method, in which a periodic boundary condition was added to the center supercell, causing it to be replicated periodically throughout space. Taking into consideration that the CuO (110) surface can be terminated by O or Cu atoms, the two models that $p(2 \times 2)$ super lattice CuO(110) slab models of the O-terminated and the Cu-terminated four atomic layers were constructed, respectively. Similarly, the $p(2 \times 2)$ super lattice CuO(111) slab models of three layers were constructed. There are four chemically distinguishable types of atoms at the CuO(111) surface: three-fold coordinated Cu atoms, four-fold coordinated Cu atoms, three-fold coordinated O atoms, and four-fold coordinated O atoms, which have been labeled as Cu_{3f} , Cu_{4f} , O_{3f} , and O_{4f} , respectively. To avoid interactions between the periodic slabs of atomic layers, a 15 Å vacuum layer was used to separate the slab models. In the calculations, the bottom layer was kept fixed while the remaining layers were allowed to fully relax. The O_2 molecules were allowed to relax. All the surface configurations are shown in Figure 13.

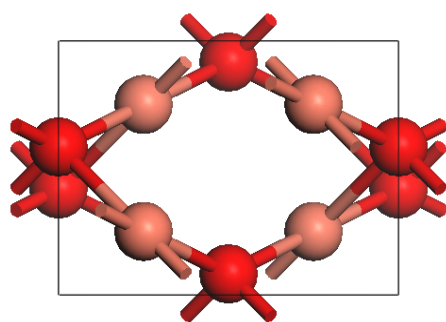


Figure 12. Schematic representation of a CuO unit cell. The salmon pink spheres denote Cu atoms, and the red spheres denote O atoms, respectively.

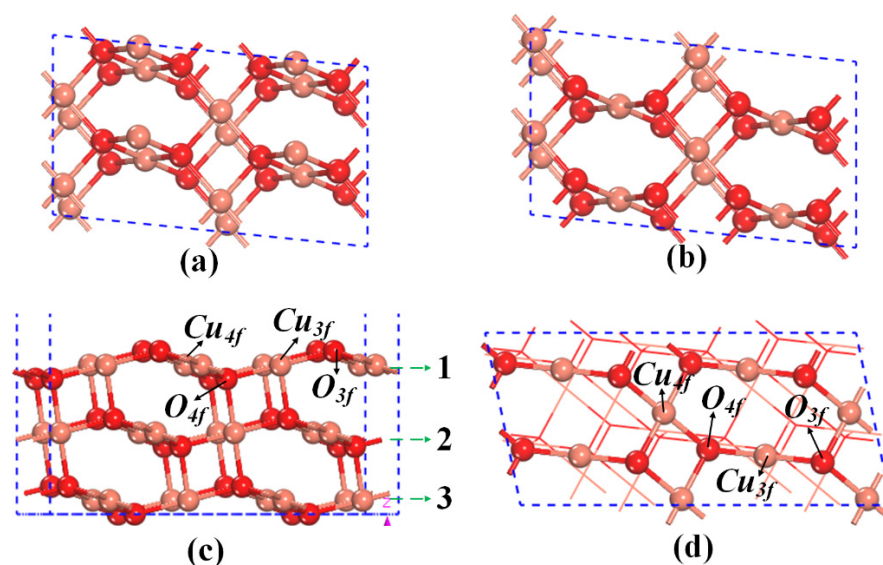


Figure 13. (a) O-terminated CuO(110) surface, (b) Cu-terminated CuO(110) surface, (c) the top view of a CuO(111) slab with different types of Cu and O atoms, and (d) the side view of a CuO(111) slab with different types of Cu and O atoms. The salmon pink spheres denote Cu atoms, and the red spheres denote O atoms, respectively.

The cut-off energy (350 eV) and the density of the Monkhorst Pack scheme k-point of $4 \times 4 \times 1$ were chosen to be sufficiently high. The kinetic energy cut-off employed in all calculations was 350 eV, and was used together with the Monkhorst Pack scheme k-point of $4 \times 4 \times 1$. The criteria for the convergence of all calculations in this work were set to (i) an energy tolerance of 2.0×10^{-5} eV/atom; (ii) a maximum force tolerance of 0.05 eV/Å; (iii) a self-consistent field tolerance of 2.0×10^{-6} eV/atom; and (iv) a maximum displacement tolerance of 0.002 Å. The following equation was used to calculate the energy barriers (E_b) of various reactions:

$$E_b = E_{TS} - E_{IS} \quad (6)$$

where E_{IS} and E_{TS} are the energies of the initial state (IS) and the transition state (TS), respectively. The oxygen vacancy creation energy (E_{vac}) is calculated by the following equation:

$$E_{vac} = E_{def} + 0.5E_{O_2} - E_{per} \quad (7)$$

where E_{def} is the energy of a defective CuO supercell containing one oxygen vacancy, and E_{O_2} is the energy of the ground state of an isolated diatomic oxygen molecule in the gas phase. E_{per} is the energy of the CuO supercell. A positive value of E_{vac} means that energy is needed to create an oxygen vacancy.

4. Conclusions

In this study, the detailed oxygen release mechanisms of CuO(110) and CuO(111) were researched at an atomic level using the DFT method. A total of five oxygen release paths on CuO(110) and CuO(111) surfaces were considered. The most favorable pathway for oxygen formation and desorption occurs on the CuO(110) surface of O-terminated. The energy barriers of oxygen formation and desorption processes are 1.89 eV and 3.22 eV, respectively, which are largely lower than other paths. The results indicate that there are active sites on the CuO surface during the oxygen release process, and they exist in pairs. The O anion diffusion processes in the CuO were further investigated. A total of eight O anion diffusion paths in CuO(110) and CuO(111) slabs were considered. The most favorable pathway for O anion diffusion is also found in the CuO(110) slab with the lowest energy barrier of 0.24 eV. By comparing both surfaces, it can be concluded that the CuO(110) surface may play a significantly important role in the oxygen release reaction due to the lowest energy barriers. On the other hand, the energy required for the subsurface oxygen to migrate to the surface oxygen vacancy is the lowest among all the O anion diffusion paths, suggesting that the O anions diffuse more easily from the lattice to the surface. In addition, the energy barriers of the O anion diffusion process are found to be substantially lower than those of the O₂ formation and desorption processes, indicating the O₂ formation and desorption are the rate-limiting steps for oxygen release from CuO, and decreasing the energy barriers of O₂ formation and desorption is the key to improving the reactivity of Cu-based oxygen carriers in CLOU. The density of states of the perfect CuO(110) slab and that with an O vacancy were studied. The results show that the TDOS for the O atoms in the CuO(110) slab shifts lower in energy after an O vacancy formation, which implies that the oxygen vacancy defect is conducive to O anion migration, which may provide an idea for increasing the reactivity of oxygen release. However, the oxygen vacancy creation energy in CuO is considerably high (7.4 eV), which means that energy is needed. Therefore, how to reduce oxygen vacancy creation energy is a topic worth studying in the future. This study would be helpful in rationalizing the development of a high-performance oxygen carrier for CLOU.

Author Contributions: Data curation, M.W. (Minjun Wang) and S.Z.; Investigation, M.W. (Minjun Wang), S.Z., M.X. and M.W. (Mengke Wang); Writing—original draft, M.W. (Minjun Wang) and M.X.; Writing—review and editing, M.W. (Minjun Wang), S.Z., M.X. and M.W. (Mengke Wang). All authors have read and agreed to the published version of the manuscript.

Funding: This research was funded by the National Natural Science Foundation of China (No. 51806089), the General Project of Natural Science Research of Jiangsu Universities (No. 18KJD470001).

Conflicts of Interest: The authors declare no conflict of interest.

References

1. Abuelgasim, S.; Wang, W.; Abdalazeez, A. A brief review for chemical looping combustion as a promising CO₂ capture technology: Fundamentals and progress. *Sci. Total Environ.* **2021**, *764*, 142892. [[CrossRef](#)]
2. Wang, M.; Liu, J.; Hu, J.; Liu, F. O₂–CO₂ Mixed Gas Production Using a Zr-Doped Cu-Based Oxygen Carrier. *Ind. Eng. Chem. Res.* **2015**, *54*, 9805–9812. [[CrossRef](#)]
3. Li, F.; Luo, S.; Sun, Z.; Bao, X.; Fan, L.-S. Role of metal oxide support in redox reactions of iron oxide for chemical looping applications: Experiments and density functional theory calculations. *Energy Environ. Sci.* **2011**, *4*, 3661–3667. [[CrossRef](#)]
4. Hossain, M.M.; Lasa, H. Chemical-looping combustion (CLC) for inherent CO₂ separations—A review. *Chem. Eng. Sci.* **2008**, *63*, 4433–4451. [[CrossRef](#)]
5. Sarshar, Z.; Sun, Z.; Zhao, D.; Kaliaguine, S. Development of Sinter-Resistant Core-Shell LaMn_xFe_{1-x}O₃@mSiO₂ Oxygen Carriers for Chemical Looping Combustion. *Energy Fuels* **2012**, *26*, 3091–3102. [[CrossRef](#)]
6. Ishida, M.; Jin, H. A Novel Chemical-Looping Combustor without NO_x Formation. *Ind. Eng. Chem. Res.* **1996**, *35*, 2469–2472. [[CrossRef](#)]
7. Mattisson, T.; Lyngfelt, A.; Leion, H. Chemical-looping with oxygen uncoupling for combustion of solid fuels. *Int. J. Greenh. Gas Control* **2009**, *3*, 11–19. [[CrossRef](#)]
8. Ahmad, A.; Al Mamun, M.A.; Al-Mamun, M.; Huque, S.; Ismail, M. LFO Perovskites as Oxygen Carriers for Chemical Looping Oxygen Uncoupling (CLOU). *J. Therm. Anal. Calorim.* **2021**, *1–9*. [[CrossRef](#)]

9. Kuang, C.; Wang, S.; Lv, S.; Cai, J.; Luo, M.; Zhao, J. Comparison of metallic oxide, natural ore and synthetic oxygen carrier in chemical looping combustion process. *Int. J. Hydrogen Energy* **2021**, *46*, 18032–18041. [[CrossRef](#)]
10. Ksepko, E. Examining SrCuO₂ as an oxygen carrier for chemical looping combustion. *J. Therm. Anal. Calorim.* **2015**, *122*, 621–633. [[CrossRef](#)]
11. Ksepko, E.; Lysowski, R. Stable Mixed Fe-Mn Oxides Supported on ZrO₂ Oxygen Carriers for Practical Utilization in CLC Processes. *Catalysts* **2021**, *11*, 1047. [[CrossRef](#)]
12. Ksepko, E.; Lysowski, R. Reactivity Study of Bimetallic Fe-Mn Oxides with Addition of TiO₂ for Chemical Looping Combustion Purposes. *Catalysts* **2021**, *11*, 1437. [[CrossRef](#)]
13. Siriwardane, R.V.; Ksepko, E.; Tian, H.; Poston, J.; Simonyi, T.; Sciazko, M. Interaction of iron–copper mixed metal oxide oxygen carriers with simulated synthesis gas derived from steam gasification of coal. *Appl. Energy* **2013**, *107*, 111–123. [[CrossRef](#)]
14. Adánez, J.; Abad, A. Chemical-looping combustion: Status and research needs. *Proc. Combust. Inst.* **2018**, *37*, 4303–4317. [[CrossRef](#)]
15. Alalwan, H.A.; Cwiertny, D.M.; Grassian, V.H. Co₃O₄ nanoparticles as oxygen carriers for chemical looping combustion: A materials characterization approach to understanding oxygen carrier performance. *Chem. Eng. J.* **2017**, *319*, 279–287. [[CrossRef](#)]
16. Vos, Y.D.; Jacobs, M.; Voort, P.; Driessche, I.V.; An, V. Development of Stable Oxygen Carrier Materials for Chemical Looping Processes—A Review. *Catalysts* **2020**, *10*, 926. [[CrossRef](#)]
17. Xu, Z.; Zhao, H.; Wei, Y.; Zheng, C. Self-assembly template combustion synthesis of a core–shell CuO@TiO₂–Al₂O₃ hierarchical structure as an oxygen carrier for the chemical-looping processes. *Combust. Flame* **2015**, *162*, 3030–3045. [[CrossRef](#)]
18. Imtiaz, Q.; Kierzkowska, A.M.; Broda, M.; Mueller, C.R. Synthesis of Cu-Rich, Al₂O₃-Stabilized Oxygen Carriers Using a Coprecipitation Technique: Redox and Carbon Formation Characteristics. *Environ. Sci. Technol.* **2012**, *46*, 3561–3566. [[CrossRef](#)] [[PubMed](#)]
19. De Diego, L.F.; García-Labiano, F.; Adánez, J.; Gayán, P.; Abad, A.; Corbella, B.M.; Palacios, J.M. Development of Cu-based oxygen carriers for chemical-looping combustion. *Fuel* **2004**, *83*, 1749–1757. [[CrossRef](#)]
20. Wang, K.; Yu, Q.; Qin, Q. Reduction Kinetics of Cu-Based Oxygen Carriers for Chemical Looping Air Separation. *Energy Fuels* **2013**, *27*, 5466–5474. [[CrossRef](#)]
21. Gayán, P.; Adánez-Rubio, I.; Abad, A.; Luis, F.; García-Labiano, F.; Adánez, J. Development of Cu-based oxygen carriers for Chemical-Looping with Oxygen Uncoupling (CLOU) process. *Fuel* **2011**, *90*, 226–238. [[CrossRef](#)]
22. Li, Z. First-principles-based microkinetic rate equation theory for oxygen carrier reduction in chemical looping. *Chem. Eng. Sci.* **2021**, *247*, 117042. [[CrossRef](#)]
23. Adánez-Rubio, I.; Abad, A.; Gayán, P.; De Diego, L.F.; García-Labiano, F.; Adánez, J. Biomass combustion with CO₂ capture by chemical looping with oxygen uncoupling (CLOU). *Fuel Process. Technol.* **2014**, *124*, 104–114. [[CrossRef](#)]
24. Adánez-Rubio, I.; Abad, A.; Gayán, P.; De Diego, L.F.; García-Labiano, F.; Adánez, J. Performance of CLOU process in the combustion of different types of coal with CO₂ capture. *Int. J. Greenh. Gas Control* **2013**, *12*, 430–440. [[CrossRef](#)]
25. Abad, A.; Adánez-Rubio, I.; Gayán, P.; García-Labiano, F.; Luis, F.; Adánez, J. Demonstration of chemical-looping with oxygen uncoupling (CLOU) process in a 1.5 kWth continuously operating unit using a Cu-based oxygen-carrier. *Int. J. Greenh. Gas Control* **2012**, *6*, 189–200. [[CrossRef](#)]
26. Qin, L.; Cheng, Z.; Fan, J.A.; Kopechek, D.; Xu, D.; Deshpande, N.; Fan, L.-S. Nanostructure formation mechanism and ion diffusion in iron–titanium composite materials with chemical looping redox reactions. *J. Mater. Chem. A* **2015**, *3*, 11302–11312. [[CrossRef](#)]
27. Su, M.A.; Cao, J.A.; Tian, X.A.; Zhang, Y.B.; Zhao, H.A. Mechanism and kinetics of Cu₂O oxidation in chemical looping with oxygen uncoupling. *Proc. Combust. Inst.* **2019**, *37*, 4371–4378. [[CrossRef](#)]
28. Li, F.; Sun, Z.; Luo, S.; Fan, L.S. Ionic diffusion in the oxidation of iron—Effect of support and its implications to chemical looping applications. *Energy Environ. Sci.* **2011**, *4*, 876–880. [[CrossRef](#)]
29. Shafiefarhood, A.; Galinsky, N.; Huang, A.P.Y.; And, Y.C.; Li, A.P.F. Fe₂O₃@La_xSr_{1-x}FeO₃ Core–Shell Redox Catalyst for Methane Partial Oxidation. *ChemCatChem* **2014**, *6*, 790–799. [[CrossRef](#)]
30. Neal, L.M.; Shafiefarhood, A.; Li, F. Dynamic Methane Partial Oxidation Using a Fe₂O₃@La_{0.8}Sr_{0.2}FeO_{3-δ} Core–Shell Redox Catalyst in the Absence of Gaseous Oxygen. *ACS Catal.* **2014**, *4*, 3560–3569. [[CrossRef](#)]
31. Cheng, Z.; Qin, L.; Guo, M.; Xu, M.; Fan, L.S. Oxygen vacancy promoted methane partial oxidation over iron oxide oxygen carriers in the chemical looping process. *Phys. Chem. Chem. Phys.* **2016**, *18*, 32418–32428. [[CrossRef](#)] [[PubMed](#)]
32. Day, M.; Tachibana, S.; Bell, J.; Lijewski, M.; Beckner, V.; Cheng, R.K. A combined computational and experimental characterization of lean premixed turbulent low swirl laboratory flames I. Methane flames. *Combust. Flame* **2012**, *159*, 275–290. [[CrossRef](#)]
33. Meng, Y. Water Gas Shift Reaction Activity on Fe (110): A DFT Study. *Catalysts* **2021**, *12*, 27.
34. Li, H.; Shi, L.; Jin, C.; Ye, R.; Zhang, R. Co and Ni Incorporated γ -Al₂O₃(110) Surface: A Density Functional Theory Study. *Catalysts* **2022**, *12*, 111. [[CrossRef](#)]
35. Bruix, A.; Margraf, J.T.; Andersen, M.; Reuter, K. First-principles-based multiscale modelling of heterogeneous catalysis. *Nat. Catal.* **2019**, *2*, 659–670. [[CrossRef](#)]
36. Meng, Y.; Liu, X.W.; Bai, M.; Guo, W.P.; Cao, D.B.; Yang, Y.; Li, Y.W.; Wen, X.D. Prediction on morphologies and phase equilibrium diagram of iron oxides nanoparticles. *Appl. Surf. Sci.* **2019**, *480*, 478–486. [[CrossRef](#)]

37. Bennett, J.W.; Huang, X.; Fang, Y.; Cwiertny, D.M.; Grassian, V.H.; Mason, S.E. Methane Dissociation on α -Fe₂O₃(0001) and Fe₃O₄(111) Surfaces: First-Principles Insights into Chemical Looping Combustion. *J. Phys. Chem. C* **2019**, *123*, 6450–6463. [[CrossRef](#)]
38. Dong, C.; Sheng, S.; Qin, W.; Lu, Q.; Zhao, Y.; Wang, X.; Zhang, J. Density functional theory study on activity of α -Fe₂O₃ in chemical-looping combustion system. *Appl. Surf. Sci.* **2011**, *257*, 8647–8652. [[CrossRef](#)]
39. Yuan, Y.; Dong, X.; Ricardez-Sandoval, L. Insights into Syngas Combustion on a Defective NiO Surface for Chemical Looping Combustion: Oxygen Migration and Vacancy Effects. *J. Phys. Chem. C* **2020**, *124*, 28359–28370. [[CrossRef](#)]
40. Feng, Y.; Wang, N.; Guo, X. Influence mechanism of supports on the reactivity of Ni-based oxygen carriers for chemical looping reforming: A DFT study. *Fuel* **2018**, *229*, 88–94. [[CrossRef](#)]
41. Feng, Y.; Guo, X. Study of reaction mechanism of methane conversion over Ni-based oxygen carrier in chemical looping reforming. *Fuel* **2017**, *210*, 866–872. [[CrossRef](#)]
42. Zhao, H.; Zhang, Y.; Wei, Y.; Gui, J. Understanding CuO-support interaction in Cu-based oxygen carriers at a microcosmic level. *Proc. Combust. Inst.* **2017**, *36*, 4069–4077. [[CrossRef](#)]
43. Wu, L.N.; Tian, Z.Y.; Kasmi, A.E.; Arshad, M.F.; Qin, W. Mechanistic study of the CO oxidation reaction on the CuO(111) surface during chemical looping combustion. *Proc. Combust. Inst.* **2021**, *38*, 5289–5297. [[CrossRef](#)]
44. Zhang, Y.; Zhao, H.; Guo, L.; Zheng, C. Decomposition mechanisms of Cu-based oxygen carriers for chemical looping with oxygen uncoupling based on density functional theory calculations. *Combust. Flame* **2015**, *162*, 1265–1274. [[CrossRef](#)]
45. Zheng, C.; Cao, J.; Zhang, Y.; Zhao, H. Insight into the Oxidation Mechanism of a Cu-Based Oxygen Carrier (Cu→Cu₂O→CuO) in Chemical Looping Combustion. *Energy Fuels* **2020**, *34*, 8718–8725. [[CrossRef](#)]
46. Mishra, A.; Li, T.; Li, F.; Santiso, E.E. Oxygen Vacancy Creation Energy in Mn-Containing Perovskites: An Effective Indicator for Chemical Looping with Oxygen Uncoupling. *Chem. Mater.* **2018**, *31*, 689–698. [[CrossRef](#)]
47. Xiang, W.; Liu, J.; Chang, M.; Zheng, C. The adsorption mechanism of elemental mercury on CuO(110) surface. *Chem. Eng. J.* **2012**, *200–202*, 91–96. [[CrossRef](#)]
48. Moreno, J.L.V.; Padama, A.A.B.; Kasai, H. A density functional theory-based study on the dissociation of NO on a CuO(110) surface. *CrystEngComm* **2014**, *16*, 2260–2265. [[CrossRef](#)]
49. Chang, Y.; Zeng, H.C. Controlled Synthesis and Self-Assembly of Single-Crystalline CuO Nanorods and Nanoribbons. *Cryst. Growth Des.* **2004**, *4*, 397–402. [[CrossRef](#)]
50. Bari, R.H.; Patil, S.B.; Bari, A.R. Spray-pyrolized nanostructured CuO thin films for H₂S gas sensor. *Int. Nano Lett.* **2013**, *3*, 12. [[CrossRef](#)]
51. Li, L.; Zhao, J.; Li, W.; Zhu, C.; Mao, L.-F.; Huang, Q. First-Principles investigation on the behavior of Pt single and triple atoms supported on monolayer CuO (110) in CO oxidation. *Appl. Surf. Sci.* **2021**, *564*, 150435. [[CrossRef](#)]
52. Massarotti, V.; Capsoni, D.; Bini, M.; Altomare, A.; Moliterni, A.G.G. X-ray powder diffraction ab initio structure solution of materials from solid state synthesis: The copper oxide case. *Z. Kristallogr.* **1998**, *213*, 259–265. [[CrossRef](#)]
53. Åsbrink, S.; Norrby, L.-J. A refinement of the crystal structure of copper(II) oxide with a discussion of some exceptional e.s.d.'s. *Acta Crystallogr. B* **1970**, *26*, 8–15. [[CrossRef](#)]
54. Zhang, R.; Liu, H.; Zheng, H.; Ling, L.; Li, Z.; Wang, B. Adsorption and dissociation of O₂ on the Cu₂O(1 1 1) surface: Thermochemistry, reaction barrier. *Appl. Surf. Sci.* **2011**, *257*, 4787–4794. [[CrossRef](#)]
55. Chadda, D.; Ford, J.D.; Fahim, M.A. Chemical energy storage by the reaction cycle cupric oxide/cuprous oxide. *Int. J. Energy Res.* **1989**, *13*, 63–73. [[CrossRef](#)]
56. Eyring, E.M.; Konya, G.; Lighty, J.S.; Sahir, A.H.; Sarofim, A.F.; Whitty, K. Chemical Looping with Copper Oxide as Carrier and Coal as Fuel. *Oil Gas Sci. Technol.* **2011**, *66*, 209–221. [[CrossRef](#)]
57. Segall, M.D.; Lindan, P.J.D.; Probert, M.J.; Pickard, C.J.; Hasnip, P.J.; Clark, S.J.; Payne, M.C. First-principles simulation: Ideas, illustrations and the CASTEP code. *J. Phys. Condens. Matter* **2002**, *14*, 2717–2744. [[CrossRef](#)]
58. Vanderbilt, D. Soft self-consistent pseudopotentials in a generalized eigenvalue formalism. *Phys. Rev. B Condens. Matter* **1990**, *41*, 7892–7895. [[CrossRef](#)]
59. Wang, M.; Liu, J.; Shen, F.; Cheng, H.; Dai, J.; Long, Y. Theoretical study of stability and reaction mechanism of CuO supported on ZrO₂ during chemical looping combustion. *Appl. Surf. Sci.* **2016**, *367*, 485–492. [[CrossRef](#)]
60. Perdew, J.P.; Burke, K.; Ernzerhof, M. Generalized Gradient Approximation Made Simple. *Phys. Rev. Lett.* **1996**, *77*, 3865–3868. [[CrossRef](#)]
61. Govind, N.; Petersen, M.; Fitzgerald, G.; King-Smith, D.; Andzelm, J. A generalized synchronous transit method for transition state location. *Comput. Mater. Sci.* **2003**, *28*, 250–258. [[CrossRef](#)]